JOURNAL OF COMPUTATIONAL PHYSICS 25, 273–296 (1977)

Numerical Solution of Problems in Unbounded Regions: Coordinate Transforms

CHESTER E. GROSCH*

Institute of Oceanography, Old Dominion University, Norfolk, Virginia 23508

AND

STEVEN A. ORSZAG†

Department of Mathematics, Massachusetts Institute of Technology, Cambridge, Massachusetts 02139

Received November 16, 1976

We investigate the utility of mappings to solve numerically problems in infinite regions. It is demonstrated by six examples that mappings are very useful if the solution being sought behaves in a simple way at infinity; otherwise, they are not particularly helpful. Solutions that vanish rapidly or approach a constant at infinity are readily treated by mapping, but solutions that oscillate out to infinity are not so amenable to these techniques. The examples investigated in detail include a one-dimensional diffusion equation, the anharmonic oscillator eigenvalue problem, the Orr–Sommerfeld eigenvalue problem for the Blasius boundary layer flow, the Falkner–Skan equation, the one-dimensional wave equation, and Burgers' equation. For these examples, it is found that an algebraic mapping of the infinite region into a finite one is best.

1. INTRODUCTION

The numerical solution of continuum problems in unbounded regions involves two essential approximations: First, the continuum must be approximated by a discrete set; and, second, the unbounded domain must be approximated by a finite domain. The first problem is the one usually studied in numerical analysis. The second has received much less attention and is the subject of the present paper. We restrict the present study to one special technique for the treatment of the point of infinity: coordinate transformation of the infinite domain into a finite region. One of the principal conclusions of the paper is that, while coordinate transformation is not always advantageous, there is a class of problems for which it is a very useful technique.

* Work supported by the Defense Advanced Research Projects Agency, monitored by the Office of Naval Research under Contract No. N00014-75-C-0777.

† Work supported by the Defense Advanced Research Projects Agency, monitored by the Office of Naval Research under Contract No. N00014-76-C-0263, ARPA Order No. 2924.

ISSN 0021-9991

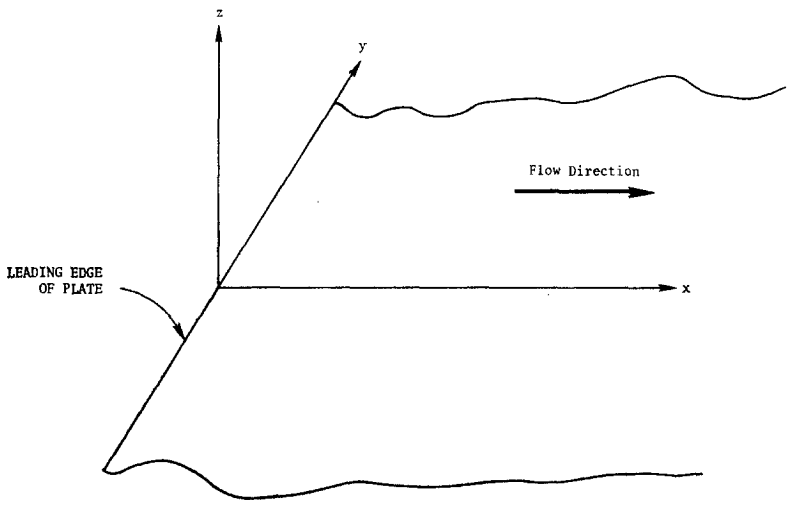

FIG. 1. Coordinate system for flow past a semi-infinite flat plate.

The present work was motivated by the problem of the numerical simulation of boundary layer flows in transition and turbulent regimes. The prototype of such flows is the flow over a semi-infinite flat plate undergoing transition to turbulence. The geometry of this three-dimensional flow (see Fig. 1) is infinite in three directions. The formulation of satisfactory boundary conditions is simplest in the y direction. On both theoretical and experimental grounds, *periodic* boundary conditions can be justified in y. On the other hand, treatment of the downstream x direction is not so simple. The mapping techniques of the present paper can *not* be used effectively for this aspect of the transition problem. Techniques for the imposition of inflow and outflow boundary conditions (which are appropriate in the x direction) will be discussed elsewhere. However, the techniques developed here are appropriate for the treatment of the z direction (normal to the boundary layer). We find that mapping techniques are successful in z because the boundary condition at $z = \infty$ is that the flow is a simple laminar free stream (in the present case, uniform flow).

The idea of mapping an infinite geometry into a finite one is not original. For example, van de Vooren and Dijkstra [1] successfully applied coordinate transformations to the numerical solution of *laminar* flow past a flat plate; Davis [2] applied similar techniques to *laminar* flow past a parabola.

We will examine the utility of mapping methods for six model problems, two of which are critical components of the boundary-layer transition study. In Section 2 we study the solution of the one-dimensional diffusion equation in a semi-infinite region. In Section 3, the eigenvalues of the quantum-mechanical harmonic oscillator are found using mappings. In Section 4, the eigenvalues of the Orr–Sommerfeld equation for the Blasius boundary layer are calculated, while in Section 5 mapping techniques are applied to the calculation of Falkner–Skan boundary-layer profiles.

The examples of Sections 6 and 7 illustrate the limitations of mapping techniques. Finally, we summarize some heuristic rules for the applicability of mappings.

2. One-Dimensional Diffusion Equation in a Semi-infinite Domain

Consider the mixed initial-boundary value problem

$$u_t = u_{xx}\,, \tag{2.1a}$$

$$u(x, t) = 0, \qquad t \leqslant 0, \tag{2.1b}$$

$$u(0, t) = \sin t, \qquad t > 0, \tag{2.1c}$$

$$u(x, t) \qquad \text{bounded as} \quad x \to \infty. \tag{2.1d}$$

One particular physical realization of these equations is the Rayleigh shear flow in the neighborhood of an oscillating flat plate [3]. As $t \to \infty$, the exact solution to (2.1) is asymptotically

$$u(x, t) \sim e^{-x/\sqrt{2}} \sin(t - x/\sqrt{2}) \qquad (t \to \infty), \tag{2.2}$$

which is just a damped wave propagating with speed $\sqrt{2}$.

The only unusual feature of the finite difference solution of (2.1) is the treatment of the unbounded domain $0 \leqslant x < \infty$. The unbounded domain leads to no difficulty if we use the one-sided approximation

$$\frac{\partial u(x, t)}{\partial t} = \frac{u(x, t) - 2u(x - h, t) + u(x - 2h, t)}{h^2}\,, \tag{2.3}$$

which is formally first-order accurate in h as $h \to 0+$. Unfortunately, explicit time-step methods for the solution of (2.3) are unstable when $\Delta t = O(h^2)$. For example, Euler time stepping requires that $\Delta t/h^2 \to 0$ as $h \to 0+$ for stability.

On the other hand, centered space differencing methods [which do yield conditional stability restrictions of the usual kind $\Delta t = O(h^2)$] lead to an unclosed set of equations. For example, the second-order semidiscrete scheme

$$\frac{\partial u(x, t)}{\partial t} = \frac{u(x + h, t) - 2u(x, t) + u(x - h, t)}{h^2} \tag{2.4}$$

involves $u(x + h, t)$ for every x, so that a finite number of equations in the same number of unknowns is never obtained in a finite x-interval.

The most obvious way to avoid the latter problem is to impose a boundary condition at an artificial boundary $x = L$, like

$$u(L, t) = 0. \tag{2.5}$$

If L is fixed, the solution to (2.4)–(2.5) does not converge as $h \to 0+$ to the solution to (2.1). However, in the double limit $L \to +\infty$, $h \to 0+$, convergence is achieved.

Another way to handle this problem is to use a nonuniform grid. Such a grid is obtained by first mapping the semi-infinite region $0 \leqslant x < \infty$ onto the finite region $0 \leqslant z < 1$ and then using the uniform grid

$$z_j = j/J, \qquad 0 \leqslant j < J. \tag{2.6}$$

The boundary condition (2.1d) becomes simply

$$u_J \text{ finite.}$$

We consider two mappings: an exponential map

$$z = 1 - e^{-x/L}, \tag{2.7}$$

and an algebraic map

$$z = x/(x + L) \tag{2.8}$$

where L is a constant scale factor. In Fig. 2 we plot z versus x for the exponential map (2.7) with various values of L. In Fig. 3 we give similar plots for the algebraic map (2.8). The points on the curves in Figs. 2 and 3 indicate the values of x with $z_j = 0.04j$ ($J = 25$). For both maps, the equivalent mesh in x is nonuniform with the most rapid variation occurring with $x \gg L$.

The exponential map (2.7) gives slightly better resolution near $x = 0$ than the algebraic map (2.8), while the algebraic map gives much better resolution than the exponential map as $x \to +\infty$. In fact,

$$x/(x + L) < 1 - e^{-x/L}$$

for all $x > 0$. Thus, if a uniform grid is used in the mapped variables and L is fixed,

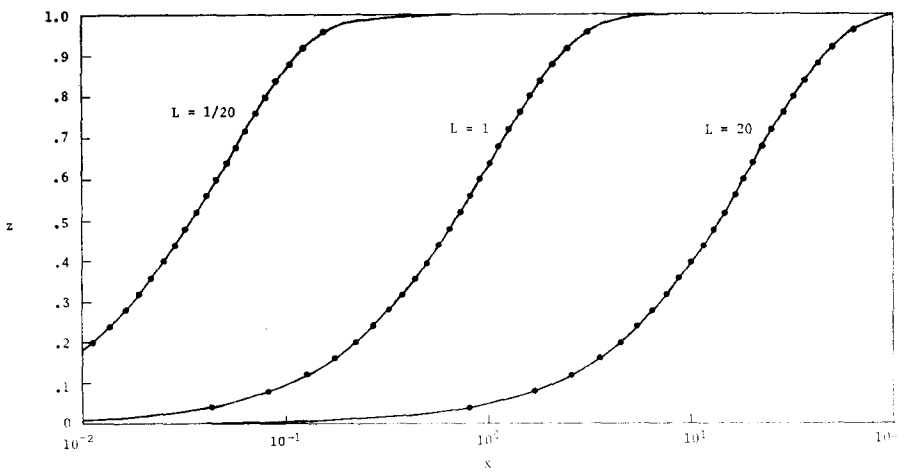

FIG. 2. Variation of z versus x for the exponential map with various values of L. The points on the curves indicate values of x with $z_j = 0.04j$.

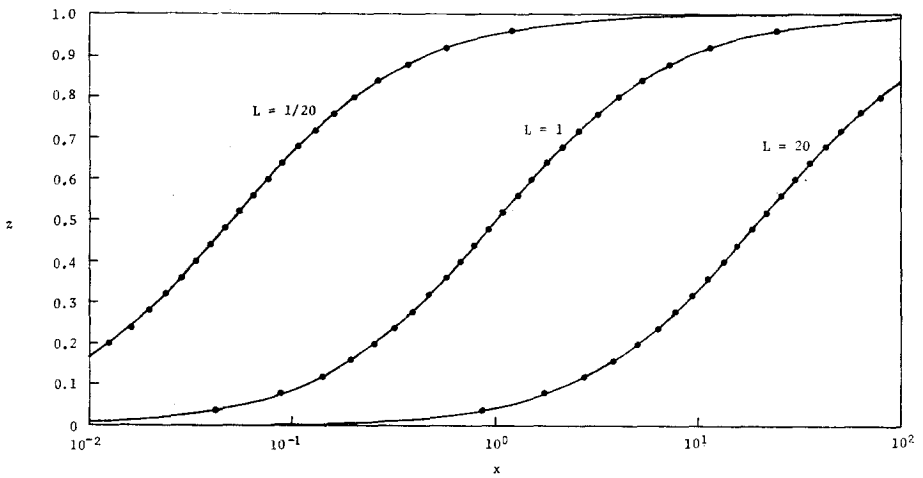

FIG. 3. Variation of z versus x for the algebraic map with various values of L. The points on the curves indicate values of x with $z_j = 0.04j$.

the grid point $z = \Delta z$ lies at a slightly *smaller* value of x with the exponential map than with the algebraic map. Conversely, the grid point $z = 1 - \Delta z$ lies at much *larger* x with the algebraic map ($x \sim L/\Delta z$) than with the exponential map ($x \sim L \ln 1/\Delta z$).

The maps (2.7) and (2.8) are especially convenient because they yield simple expressions for derivatives. With the exponential map (2.7), derivatives with respect to x become

$$\frac{\partial u(x, t)}{\partial x} = \frac{1 - z}{L} \frac{\partial u(z, t)}{\partial z}, \tag{2.9a}$$

$$\frac{\partial^2 u(x, t)}{\partial x^2} = \frac{1}{L^2} (1 - z) \frac{\partial}{\partial z} (1 - z) \frac{\partial u(z, t)}{\partial z}. \tag{2.9b}$$

With the algebraic map (8), derivatives with respect to x become

$$\frac{\partial u(x, t)}{\partial x} = \frac{(1 - z)^2}{L} \frac{\partial u(z, t)}{\partial z}, \tag{2.10a}$$

$$\frac{\partial^2 u(x, t)}{\partial x^2} = \frac{1}{L^2} (1 - z)^2 \frac{\partial}{\partial z} (1 - z)^2 \frac{\partial u(z, t)}{\partial z}. \tag{2 10b}$$

With these transformations and centered space differencing of all z derivatives, a closed set of equations is obtained for the numerical solution of problem (2.1).

Let us now compare some numerical results for the solution of (2.1) using the three methods discussed above: restriction to $x \leqslant L$, exponential mapping (2.7), and algebraic mapping (2.8). In general, there are two kinds of numerical error: truncation error and mapping error. In the case of the solution using the restricted

x-interval $0 \leqslant x < L$, the truncation error is of order h^2 and the mapping error due to neglect of the interval $L \leqslant x < \infty$ and imposition of $u(L, t) = 0$ is of order $\exp(-L/\sqrt{2})$ [see (2.2)]. It turns out that, in order to obtain an absolute error of 10^{-3} in the asymptotic solution (2.2) for $t \to \infty$ at $x = 1$, numerical solutions using the restricted-domain method require $L \gtrsim 10$ and $h \lesssim \frac{1}{8}$, or a total of at least 50 grid points (see Table I).

TABLE I

Errors in the Numerical Solution of the Rayleigh Shear Flow at $x = 1.0$ as $t \to \infty$.

			L				
Mapping	N	0.5	1.0	2.5	$2\sqrt{2}$	5.0	10.0
Restricted	21	—	0.5	5.7×10^{-2}	—	2.0×10^{-3}	5.1×10^{-3}
domain	41	—	0.5	5.7×10^{-2}	—	1.7×10^{-3}	1.3×10^{-3}
	81	—	0.5	5.7×10^{-2}	—	1.7×10^{-3}	3.2×10^{-4}
	101	—	0.5	5.7×10^{-2}	—	1.7×10^{-3}	2.0×10^{-4}
	201	—	0.5	5.7×10^{-2}	—	1.7×10^{-3}	6.6×10^{-5}
Exponential	21	7.5×10^{-2}	3.1×10^{-3}	2.3×10^{-4}	3.4×10^{-4}	1.1×10^{-3}	4.6×10^{-3}
	31	4.8×10^{-2}	1.8×10^{-3}	1.7×10^{-4}	1.5×10^{-4}	5.7×10^{-4}	2.0×10^{-3}
	41	4.1×10^{-2}	1.2×10^{-3}	1.2×10^{-4}	8.3×10^{-5}	3.1×10^{-4}	1.0×10^{-3}
	61	3.0×10^{-2}	6.7×10^{-4}	2.9×10^{-5}	3.6×10^{-5}	1.3×10^{-4}	5.1×10^{-4}
	81	2.5×10^{-2}	4.5×10^{-4}	1.6×10^{-5}	2.1×10^{-5}	8.8×10^{-5}	2.9×10^{-4}
Algebraic	21	9.5×10^{-4}	4.7×10^{-4}	5.4×10^{-4}	—	1.4×10^{-3}	4.2×10^{-3}
	31	4.1×10^{-4}	2.4×10^{-4}	3.0×10^{-4}	—	5.6×10^{-4}	1.9×10^{-3}
	41	1.9×10^{-4}	1.5×10^{-4}	1.4×10^{-4}	—	3.2×10^{-4}	1.1×10^{-3}
	61	1.0×10^{-4}	7.0×10^{-5}	1.1×10^{-4}	—	1.6×10^{-4}	5.2×10^{-4}
	81	5.0×10^{-4}	4.0×10^{-5}	3.7×10^{-5}	—	9.0×10^{-5}	2.6×10^{-4}

The algebraic map allows accurate results to be obtained much more efficiently. For example, to achieve an error of less than 10^{-3} as $t \to \infty$ at $x = 1$ requires less than 15 grid points using the algebraic map (2.8) with $L = 1$ (see Table I).

The results given in Table I show that the algebraic map gives a much better representation of the solution for large x than the results obtained by restricting the domain or the exponential map. The reason for this behavior is simply that the amplitude of the solution (2.1) is

$$f_1(z) = e^{-Lz/[\sqrt{2}(1-z)]}$$

in terms of the algebraic map (2.8), while it is

$$f_2(z) = (1 - z)^{L/\sqrt{2}}$$

in terms of the exponential map (2.7). The function $f_1(z)$ and all its derivatives vanish at $z = 1$. On the other hand, $f_2'(1) = \infty$ (for $L = 1$), which induces a relatively large error when the exponential map is used. Observe from Table I that the errors obtained using the exponential map do *not* decrease as h^2 as $h \to 0+$ when $L < 2\sqrt{2}$. When $L = 2\sqrt{2}$, $f_2(z)$ and all its derivatives are finite at $z = 1$; the error is less than 10^{-4} as $t \to \infty$ at $x = 1$ with only about 35 points. *In general, if the exact solution or one of its z-derivatives is singular at* $z = 1$ (*or* $x = \infty$), *large numerical errors result.*

3. Eigenvalues of the Quantum-Mechanical Harmonic Oscillator

The eigenvalues λ of the Hermite equation

$$u'' - \tfrac{1}{4}x^2u = -\lambda u, \qquad u \text{ bounded as } \quad |x| \to \infty \tag{3.1}$$

are $\lambda = n + \frac{1}{2}$ ($n = 0, 1, 2,...$). The corresponding eigenfunctions are the Hermite functions $\exp(-\frac{1}{4}x^2)\,\mathrm{He}_n(x)$, where $\mathrm{He}_0(x) = 1$, $\mathrm{He}_1(x) = x$, $\mathrm{He}_2(x) = x^2 - 1$, and so on. If n is even the eigenfunctions are even functions of x; if n is odd, the eigenfunctions are odd functions. We shall only study the even eigenvalues and eigenfunctions.

The numerical solution of (3.1) requires a method for handling the boundary conditions at $\pm\infty$. Here we compare two methods applied to the determination of the even modes. In the first method, we assume that the function u is a function of x^2 alone and require

$$u(L) = 0 \tag{3.2a}$$

for some large L. In the second method, we make the algebraic map

$$z = 2[x^2/(x^2 + L^2)] - 1 \tag{3.2b}$$

and seek the solution as a bounded function of z for $-1 \leqslant z < 1$.

For both methods of handling the boundary conditions at ∞, we use Chebyshev series [4] to represent the eigenfunction $u(x)$. In the first method, $u(x)$ is represented as

$$u(x) = \sum_{n=0}^{N} a_n T_{2n}(x/L), \tag{3.3}$$

and the boundary condition (3.2a) is applied; in the second method, $u(x)$ is represented in terms of the mapped variable (3.2b) as

$$u(x) = \sum_{n=0}^{N} a_n T_n(z). \tag{3.4}$$

Here $T_n(y)$ is the Chebyshev polynomial of degree n defined by

$$T_n(\cos\theta) = \cos n\theta.$$

TABLE II

Convergence of Approximations to the Eigenvalue $\lambda = 4.5$ of the Quantum-Mechanical Harmonic Oscillator using $N + 1$ Chebyshev Polynomials

Map	L	N	λ
Truncation	4.0	10	5.20628 14857
$-L \leqslant x \leqslant L$	4.0	30	5.20628 12800
	8.0	10	4.57205 38006
	8.0	20	4.50000 00394
	8.0	30	4.50000 00395
	16.0	20	4.56679 36320
	16.0	30	4.50000 17110
	32.0	30	5.47165 94003
Algebraic	4.0	20	4.50029 00880
$z = 2\dfrac{x^2}{x^2 + L^2} - 1$	4.0	30	4.49999 99641
	8.0	10	4.56858 45536
	8.0	20	4.50002 73879
	8.0	30	4.49999 99985
	16.0	20	4.50000 02905
	16.0	30	4.50000 00000
	32.0	10	4.49656 47888
	32.0	20	4.49999 98895
	32.0	30	4.50000 00000
	64.0	20	4.49999 99898
	128.0	20	4.49999 96979
	256.0	20	4.62092 09932

TABLE III

Values of the Eigenvalues λ of the Quantum-Mechanical Harmonic Oscillator Obtained with the Algebraic Map and $N = 20$ (21 Chebyshev Polynomials)

	λ		
L	0.5	2.5	4.5
1	0.5000 0171	2.5016 8050	4.4889 8957
2	0.5000 0004	2.5001 2172	4.4968 0153
4	0.5000 0000	2.5000 0347	4.5002 9009
8	0.5000 0000	2.5000 0000	4.5000 2739
16	0.5000 0000	2.5000 0000	4.5000 0029
32	0.5000 0000	2.5000 0000	4.4999 9989
64	0.5000 0000	2.5000 0000	4.4999 9999
128	0.5000 0000	2.5000 0000	4.4999 9970
256	0.5000 0680	2.5040 4612	4.6209 2099
512	0.5046 4052	2.7962 9628	6.3984 1320

The details of the application of Chebyshev series to the numerical solution of ordinary and partial differential equations are given in [4, 5].

In Tables II and III, we present numerical results obtained by the methods described above for the even modes having exact eigenvalues $\frac{1}{2}, \frac{5}{2}, \frac{9}{2}$. It should be apparent that the algebraic mapping achieves high accuracy much more efficiently than does simple truncation of the infinite interval. Notice that for a given number of Chebyshev polynomials N there is an optimal choice of scale L that gives the most accurate result. Also, observe that for fixed L there is rapid (faster than algebraic) convergence of the eigenvalues as $N \to \infty$ in both methods. This is a general property of Chebyshev expansions. However, when truncation to $|x| \leqslant L$ is used the eigenvalues converge to the wrong answer unless the simultaneous limit $L \to \infty$ is also taken.

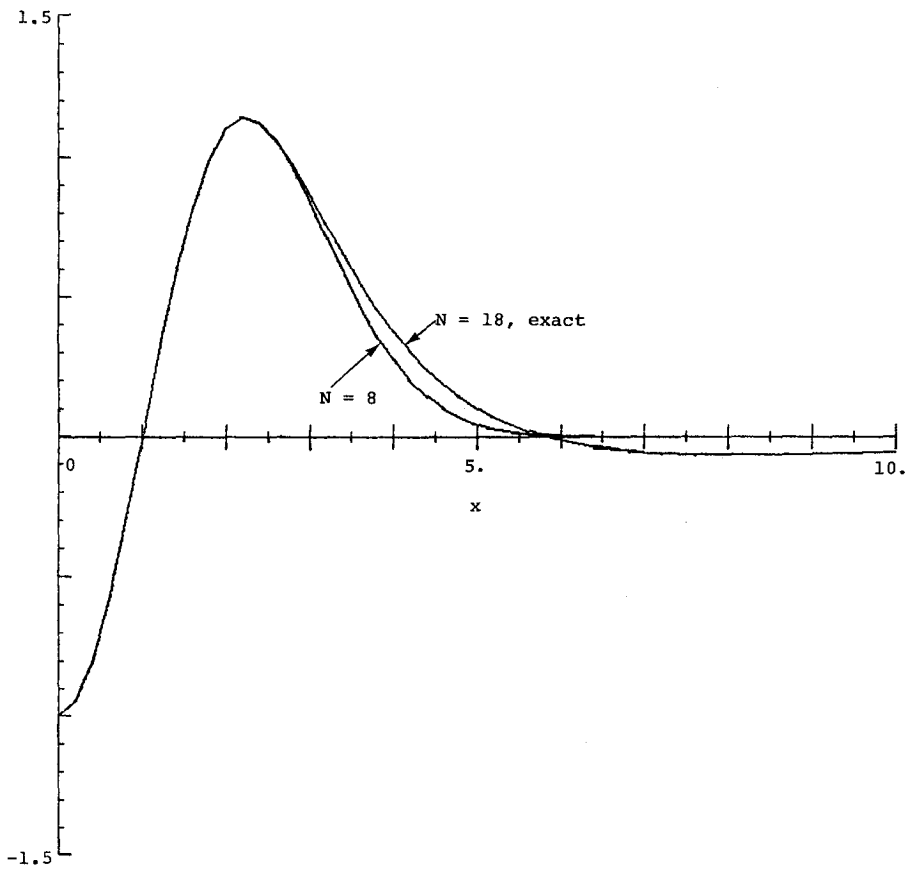

FIG. 4. Plot of the approximate and exact eigenfunctions for the eigenvalue $\frac{5}{2}$ of the quantum-mechanical harmonic oscillator obtained using the algebraic map (3.2b) with $L = \sqrt{2}$. The Chebyshev approximation (3.3) with $N = 18$ is not distinguishable from the exact eigenfunction $u(x) = -(1 - x^2)\exp(-x^2/4)$.

In Fig. 4, we plot the eigenfunction corresponding to the eigenvalue $\frac{5}{2}$ obtained using the algebraic mapping (3.3) for various numbers of Chebyshev polynomials N. The eigenfunctions are all normalized by $u(0) = -1$. Here the exact eigenfunction of (3.1) with $E = \frac{5}{2}$ is $-(1 - x^2)\exp(-\frac{1}{4}x^2)$. Notice the very rapid convergence to the exact eigenfunction as N increases.

4. Orr–Sommerfeld Equation for Blasius Flow

The Orr–Sommerfeld equation governs two-dimensional linear disturbances to incompressible parallel shear flows. We assume that the (dimensionless) undisturbed flow velocity is $U(z)\hat{x}$, where $\hat{x}$ is a unit vector in the x-direction and that the z-component of the perturbation velocity is proportional to the real part of

$$w(z)e^{i\alpha(x-ct)},$$

where α, the longitudinal wavenumber, is assumed real and c (usually complex) is the phase speed of the disturbance propagating in x. If $\mathrm{Im}(c) > 0$, the disturbance grows in time and the flow is unstable. It may be shown that the linearized, incompressible, Navier–Stokes equations can be reduced to the Orr–Sommerfeld equation

$$\left(\frac{d^2}{dz^2} - \alpha^2\right)^2 w = i\alpha R\left[(U(z) - c)\left(\frac{d^2}{dz^2} - \alpha^2\right)w - U''(z)w\right], \tag{4.1}$$

where R is the Reynolds number. On rigid no-slip walls, the perturbation velocity must satisfy

$$w = w' = 0. \tag{4.2}$$

The problem (4.1) with the homogeneous boundary conditions (4.2) is an eigenvalue problem for the phase speed c, assuming α is given.

The laminar flow over a flat plate $z = 0$, as in Fig. 1, satisfies the conditions of the preceding paragraph except for a slow variation in x which we neglect; $U(z)$ is the Blasius velocity profile which is determined by equations summarized in Section 5. Linearized disturbances to the Blasius flow are governed by (4.1) with the boundary conditions (4.2). As $z \to \infty$, the disturbance should remain bounded; it may be shown that this condition becomes

$$w(z) \sim e^{-\alpha z} \qquad (z \to \infty) \tag{4.3}$$

if R is large, c is not close to 1, and $\mathrm{Im}\,(\alpha c) > 0$.

The problem is to solve numerically the eigenvalue problem (4.1)–(4.3) in the region $0 \leqslant z < \infty$. We will compare several methods for handling the boundary condition at ∞. First, the region may be truncated to the region $0 \leqslant z < L$ with the artifical boundary conditions

$$w(L) = w'(L) = 0 \tag{4.4}$$

imposed on the finite lid $z = L$. Second, the asymptotic behavior (4.3) may be used to infer the improved boundary condition

$$w'(L) + \alpha w(L) = 0 \tag{4.5}$$

on $z = L$. The other methods we will compare use the exponential and algebraic mappings (2.7)–(2.8) of the semi-infinite region $0 \leqslant z < \infty$ into a finite domain.

The exponential map

$$Z = 1 - 2e^{-z/L} \tag{4.6}$$

transforms the region $0 \leqslant z < \infty$ into $-1 \leqslant Z < 1$. Two types of boundary conditions will be applied at $Z = 1$ ($z = \infty$):

$$w(Z) = 0(1) \qquad (Z \to 1-) \tag{4.7}$$

and

$$w|_{Z=1} = dw/dZ|_{Z=1} = 0. \tag{4.8}$$

The algebraic map

$$Z = 2[z/(L + z)] - 1 \tag{4.9}$$

also transforms $0 \leqslant z < \infty$ into $-1 \leqslant Z < 1$. Three kinds of boundary conditions will be applied at $Z = 1$:

$$w(Z) = O(1) \qquad (Z \to 1-), \tag{4.10}$$

$$w|_{Z=1} = 0, \tag{4.11}$$

and

$$w|_{Z=1} = dw/dZ|_{Z=1} = 0. \tag{4.12}$$

We have computed the eigenvalues of the Orr–Sommerfeld equation for these various cases by expansion of w in a series of Chebyshev polynomials [4], the eigenvalues being found by matrix eigenvalue methods [6]. Comparisons between the methods are given for the case $R = 580$, $\alpha = 0.179$, a case previously studied in some detail [7, 8]. Results are given in Table IV only for the single unstable eigenvalue (Im $c > 0$) for this choice of R, α. Here N is the number of Chebyshev polynomials used to represent the modes. High resolution numerical calculations yield the value

$$c = 0.36412286 + i\,0.00795972 \tag{4.13}$$

to eight decimal places. In all cases, $w(0) = w'(0) = 0$ at the rigid wall $z = Z = 0$.

Comparison of cases 1–4 with the "exact" solution (4.13) shows that the error in c incurred by truncation to $z \leqslant L$ is of order $e^{-2\alpha L}$; also, for fixed L, the convergence with increasing N is very rapid, consistent with the expected infinite-order rate of convergence of Chebyshev series [4]. Cases 5 and 6 show that the "improved" boundary condition (4.5) does not help, at least for the values of N used in the present calcula-

TABLE IV

Eigenvalues of the Orr–Sommerfeld Equation for Blasius Flow, $R = 580$, $\alpha = 0.179$

Case	Mapping	Boundary Conditions at $z = \infty$	L	N (number of Chebyshev modes)	c
1	Truncation	$w(L) = w'(L) = 0$	10	44	0.37887 7 + i0.00025 0
2		$w(L) = w'(L) = 0$	20	44	0.36455 7 + i0.00777 3
3		$w(L) = w'(L) = 0$	20	46	0.36455 1 + i0.00778 1
4		$w(L) = w'(L) = 0$	30	44	0.36399 6 + i0.00788 8
5		$w'(L) + \alpha w(L) = 0$	20	44	0.36021 3 + i0.00667 1
6		$w'(L) + \alpha w(L) = 0$	30	44	0.36404 1 + i0.00811 3
7	Exponential	$w(1) = 0(1)$	1	42	0.34858 0 + i0.01312 9
8		$w(1) = 0(1)$	1	46	0.34961 1 + i0.01285 6
9		$w(1) = w'(1) = 0$	1	46	0.38378 9 − i0.00276 6
10		$w(1) = w'(1) = 0$	1	70	0.37853 1 + i0.00047 1
11	Algebraic	$w(1) = 0(1)$	1	26	0.36414 7 + i0.00800 7
12		$w(1) = 0(1)$	1	34	0.36412 1 + i0.00795 76
13		$w(1) = 0(1)$	1	42	0.36412 288 + i0.00795 975
14		$w(1) = w'(1) = 0$	1	42	0.36412 325 + i0.00795 894
15		$w(1) = w'(1) = 0$	1	60	0.36412 285 + i0.00795 973
16		$w(1) = 0$	1	42	0.36412 287 + i0.00795 976

tions. In fact, use of (4.5) does improve the results if N is large. We do not enter into these comparisons further because they are not central to the present paper.

The results of cases 7–10 for the exponential map are very disappointing. With the upper boundary condition (4.7), the convergence rate is roughly like $1/N$; the boundary conditions (4.8) do not help. This behavior is explained as follows. The asymptotic behavior (4.3) implies that, in the mapped coordinate (4.6),

$$w \sim (1 - Z)^{\alpha L} \qquad (Z \to 1-). \tag{4.14}$$

Since $\alpha L = 0.179$ for cases 7–10, it follows that w has a cusp singularity at $Z = 1$. This singularity in the derivative of w at $Z = 1$ slows the convergence of the Chebyshev series representation of w. The boundary conditions (4.8) are inconsistent with the asymptotic behavior (4.3) since $\lim_{Z \to 1-} w'(Z) = \infty$; nevertheless, convergence to the correct eigenvalue seems to be obtained, but the inconsistency destroys the rapid convergence properties of Chebyshev series.

On the other hand, the algebraic map (4.9) works remarkably well. Comparison of cases 11–16 with the "exact" result (4.13) shows that extremely rapid convergence is achieved at low values of N. The reason is that in the algebraically mapped coordinate (4.3) becomes

$$w \sim e^{-\alpha L(1+Z)/(1-Z)} \qquad (Z \to 1-).$$

Thus, w and *all* its derivatives with respect to Z approach 0 as $Z \to 1-$. In contrast to the exponential map, the algebraic map gives nicely behaved solutions as $Z \to 1-$.

5. Application to the Falkner–Skan Equation

Consider the semi-infinite flat plate shown in Fig. 1 in which the uniform inflow at $x = 0$ is tilted at an angle $\frac{1}{2}\beta\pi$ with respect to the plate. It can be shown that the x component of the velocity at $z = \infty$ is

$$U(x) = U_0(x/l)^m. \tag{5.1}$$

Here U_0 is the free stream velocity at $x = 0$, l is a length scale, and

$$m = \beta/(2 - \beta). \tag{5.2}$$

If $\beta > 0$, the flow is accelerated along the plate; this case can also be interpreted as the flow over a wedge with an included angle of $\beta\pi$. If $\beta < 0$, the flow is decelerated and the flow is just the same as occurs on the underside of the plate when $\beta > 0$. Finally, if $\beta = 0$, the flow is parallel to the plate and neither accelerates nor decelerates.

The requirement that the velocity at the surface of the plate be zero leads to the formation of a boundary layer in the immediate vicinity of the plate. This boundary layer flow problem is solved by introducing the similarlity variable

$$\eta = z[\tfrac{1}{2}(m + 1)\, U(x)/\nu x]^{1/2} \tag{5.3}$$

and a stream function $\psi(x, z)$ related to the x and z components of the velocity, u and v by

$$u = \psi_z\,, \tag{5.4}$$

$$v = -\psi_x\,. \tag{5.5}$$

If we set

$$\psi = [(2/(m + 1))\, \nu x U(x)]^{1/2} f(\eta), \tag{5.6}$$

where ν is the kinematic viscosity, the laminar boundary layer equations reduce to the Falkner–Skan equation

$$f''' + ff'' + \beta[1 - (f')^2] = 0. \tag{5.7}$$

Here primes indicate differentiation with respect to η. The boundary conditions for this equation are as follows:

(i) The requirement of zero velocity on the plate gives

$$f(0) = f'(0) = 0. \tag{5.8}$$

TABLE V

Errors in Solution of the Falkner–Skan Equation Using 11 Grid Points

Method	L	Error in $f'(1)$
	($\beta = 0$)	($f'(1) = .4606$)
Restricted domain	1.0	5.4×10^{-1}
	2.5	5.2×10^{-2}
	5.0	1.3×10^{-4}
	7.5	[a]
	10.	[a]
Exponential map	1.0	-1.1×10^{-1}
	2.5	-1.2×10^{-1}
	5.0	-1.0×10^{-1}
	7.5	-8.2×10^{-2}
	10.	-6.9×10^{-2}
Algebraic map	1.0	5.8×10^{-6}
	2.5	-4.7×10^{-7}
	5.0	-2.8×10^{-6}
	7.5	-4.0×10^{-6}
	10.	-6.7×10^{-5}
	$\beta = -.1$	$f'(1) = .3630$
Restricted domain	5.0	4.2×10^{-4}
	7.5	[a]
Exponential map	5.0	-8.8×10^{-2}
	7.5	-7.3×10^{-2}
Algebraic map	5.7	-4.6×10^{-6}
	7.5	-6.4×10^{-6}
	$\beta = .1$	$f'(1) = .5274$
Restricted domain	2.5	3.2×10^{-2}
	5.0	1.4×10^{-1}
	7.5	[a]
Exponential map	2.5	-1.3×10^{-6}
	5.0	-1.1×10^{-1}
	7.5	-8.7×10^{-2}
Algebraic map	2.5	-5.5×10^{-6}
	5.0	-1.1×10^{-5}
	7.5	-1.6×10^{-5}

[a] No acceptable (monotonic) solution.

(ii) The requirement that the flow velocity approach the free stream value as $z \to \infty$ implies

$$f'(\eta) \to 1 \qquad (\eta \to +\infty). \tag{5.9}$$

Properties of the solutions to this boundary value problem have been extensively investigated [9].

We solved (5.7)–(5.9) numerically using a fourth-order Runge–Kutta shooting method together with the mappings introduced earlier. Some results of our computations using only 11 grid points (!) are given in Table V. In this table, we give the errors in the approximate solution for $f'(\eta)$ at $\eta = 1$ for the restricted domain, exponential mapping, and algebraic mapping for a variety of choices of scale L for fixed total number of grid points. It is apparent from these results that the algebraic mapping allows substantial economies in the numerical solution of the Falkner–Skan equation. As in Section 4, the efficiency of the mapping methods is most important in the context of multidimensional numerical hydrodynamics, where economy in resolution is vital.

6. Wave Equation

In this section we study the application of mapping to the problem

$$\begin{aligned} u_{tt} &= u_{xx} \qquad (0 < x < \infty,\ t > 0), \\ u(0, t) &= f(t) \qquad (t > 0), \\ u(x, 0) &= u_t(x, 0) = 0 \qquad (0 < x < \infty). \end{aligned} \tag{6.1}$$

The exact solution to this problem is

$$\begin{aligned} u(x, t) &= f(t - x), \qquad x < t, \\ &= 0, \qquad\qquad x \geqslant t, \end{aligned} \tag{6.2}$$

which represents an outgoing wave at $x = +\infty$.

If the semi-infinite interval $0 \leqslant x < \infty$ is replaced by the finite interval $0 \leqslant x = L$, boundary conditions must be applied at $x = L$. If the boundary condition that is applied is simply

$$u(L, t) = 0,$$

waves reflect from the boundary; the exact solution to (6.1) on the interval $0 \leqslant x \leqslant L$ with $u(L, t) = 0$ is

$$u(x, t) = \sum_{n=0}^{\infty} [\hat{f}(t - x - 2nL) - \hat{f}(t + x - 2(n + 1)L)], \tag{6.3}$$

where $\hat{f}(s) = f(s)$ if $s > 0$ and $\hat{f}(s) = 0$ if $s \leqslant 0$. The solution (6.3) consists of the

original outgoing wave (6.2) together with reflected waves that begin to appear at $t = nL$, $n = 1, 2, \ldots$. If x is near 0 the solution (6.3) is a good approximation to the exact solution (6.2) only for $t < 2L$ when the first reflected wave arrives at $x = 0$.

There are other boundary conditions that can be applied at $x = L$ that do not yield reflected waves. If we set

$$u_t + u_x = 0 \tag{6.4}$$

at $x = L$, the exact solution (6.2) is recovered. However, we do not enter into a discussion of radiation boundary conditions like (6.4) here; a full discussion of them will be given elsewhere.

The mappings (2.7), (2.8) can also be applied to the wave problem (6.1). For example with the algebraic map (2.8), (6.1) becomes

$$\frac{\partial^2 u}{\partial t^2} = \frac{(1-z)^2}{L^2}\frac{\partial}{\partial z}(1-z)^2\frac{\partial u}{\partial z} \qquad (0 \leqslant z < 1,\ t \geqslant 0). \tag{6.5}$$

To analyze these methods, we note that there are basically two kinds of errors in the numerical solution: first, there are local truncation errors in the representation of the wave propagating through x; and, second, there are the reflected waves from the artificial boundary at $z = 1$. In practice, the first kind of error is kept to within a few percent with a second-order difference scheme so long as the grid resolution Δx satisfies

$$\Delta x < \lambda/M, \tag{6.6}$$

where λ is the wavelength and M is a number of order 10; roughly speaking, at least 10 grid points per wavelength are required for an accurate calculation.

The error due to the reflected waves is more serious; when the first reflected wave arrives the solution is completely wrong! It turns out in practice that waves are reflected appreciably either from the boundary at $x = L$ if there is no map or, with a map, from the points x at which

$$\Delta x \gtrsim \tfrac{1}{2}\lambda. \tag{6.7}$$

When the local grid spacing gets larger than roughly $\frac{1}{2}\lambda$, as it must for z close to 1, waves can no longer be resolved on the mapped grid. Since

$$dx/dz = L/(1-z)^{\alpha},$$

where $\alpha = 1$ for the exponential map (2.7) and $\alpha = 2$ for the algebraic map (2.8) and since the grid spacing in z is $\Delta z = 1/N$, it follows that $\Delta x = \frac{1}{2}\lambda$ when

$$1 - z = (2L/N\lambda)^{1/\alpha}.$$

Thus, appreciable reflection of waves occurs near

$$x = (\tfrac{1}{2}N\lambda L)^{1/2}, \tag{6.8}$$

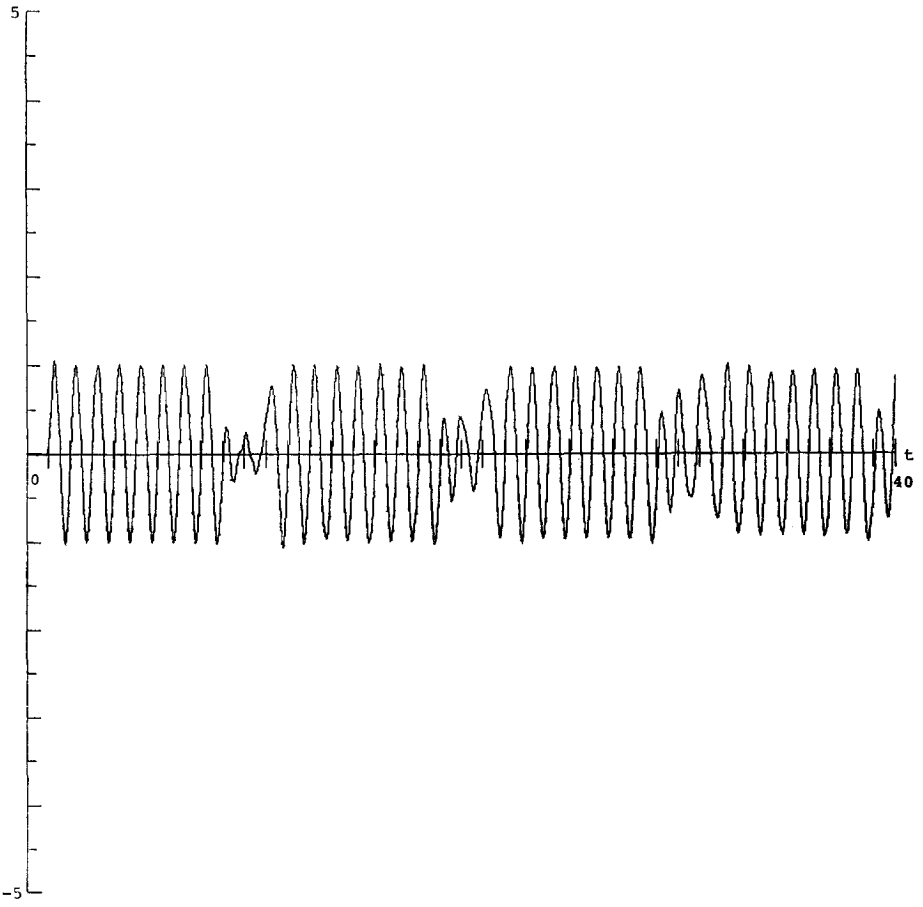

FIG. 5. Plot of the solution to the wave equation (6.1) at $x = 1$ as a function of t using the restricted domain method with $L = 5$.

with the algebraic map (assuming $2L \ll N\lambda$) and near

$$x = L \ln(N\lambda/2L) \tag{6.9}$$

with the exponential map. These results are consistent with the numerical results plotted in Figs. 5–7.

Now we pose the following question. Suppose that N, the number of grid points, is fixed and that we wish to calculate k wavelengths of the solution (6.2) accurately for as long a time as possible. Since the scale of the maps is a free parameter, we can choose L to maximize the time interval of accuracy. The question is: For how long do the various mappings maintain an accurate solution? We analyze three cases: (i) $z = x/L$. In this case, the calculation is accurate until roughly $t = 2L$ when the

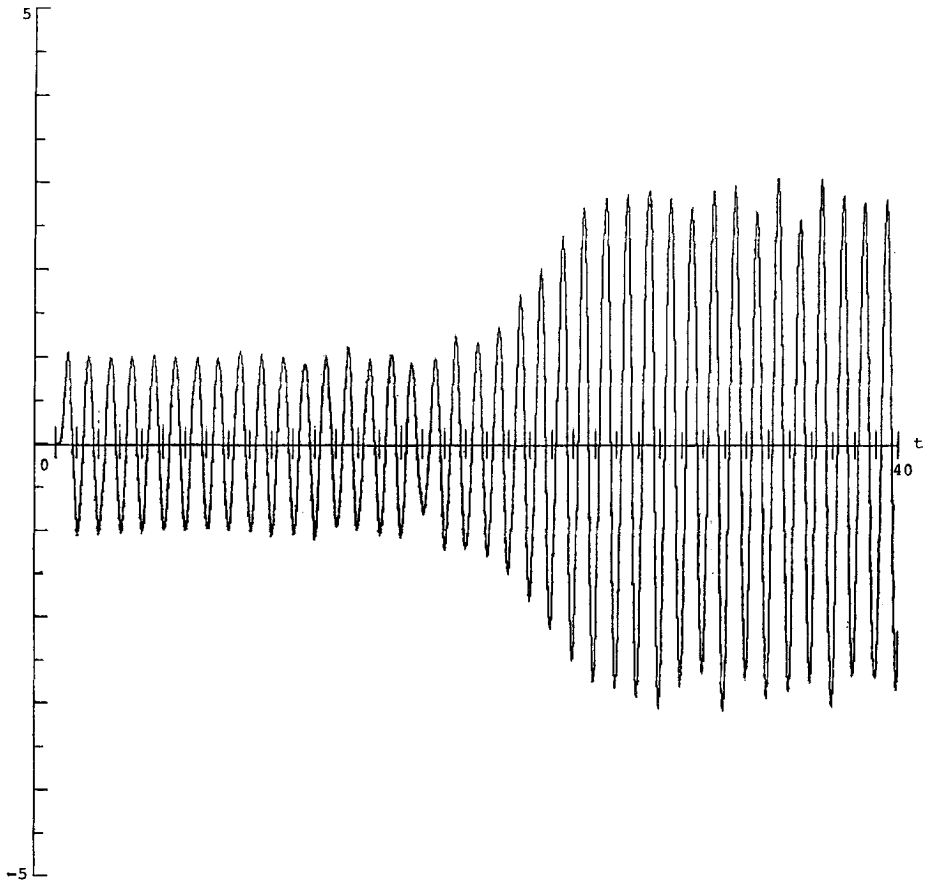

FIG. 6. Plot of the solution to the wave equation (6.1) at $x = 1.25$ as a function of t using the algebraic map with $L = 5$.

first reflected wave arrives (assuming $L \gg k\lambda$). Since we must choose $L/N = \Delta x \lesssim \lambda/M$ (where $M \approx 10$) it follows that

$$t_{\text{accuracy}} = 2\lambda N/M.$$

(ii) $z = x/(x + L)$. In this case (6.8) shows that the first reflected wave arrives at $x = 0$ at $t = (2N\lambda L)^{1/2}$. However, small local truncation error for the first k wavelengths about $x = 0$ requires that, for z near 0, $\Delta x < \lambda/M$. Thus, we must also require $L \lesssim N\lambda/M$. Thus, the optimal time of accuracy is roughly

$$t_{\text{accuracy}} = (2/M)^{1/2} N\lambda.$$

(iii) $z = 1 - e^{-x/L}$. Equation (6.9) implies that the first reflected waves reach $x = 0$ at $t = 2L \ln(N\lambda/2L)$. As in (i) and (ii) above, $L \lesssim N\lambda/M$ so that

$$t_{\text{accuracy}} = (2/M)\, N\lambda \ln(M/2).$$

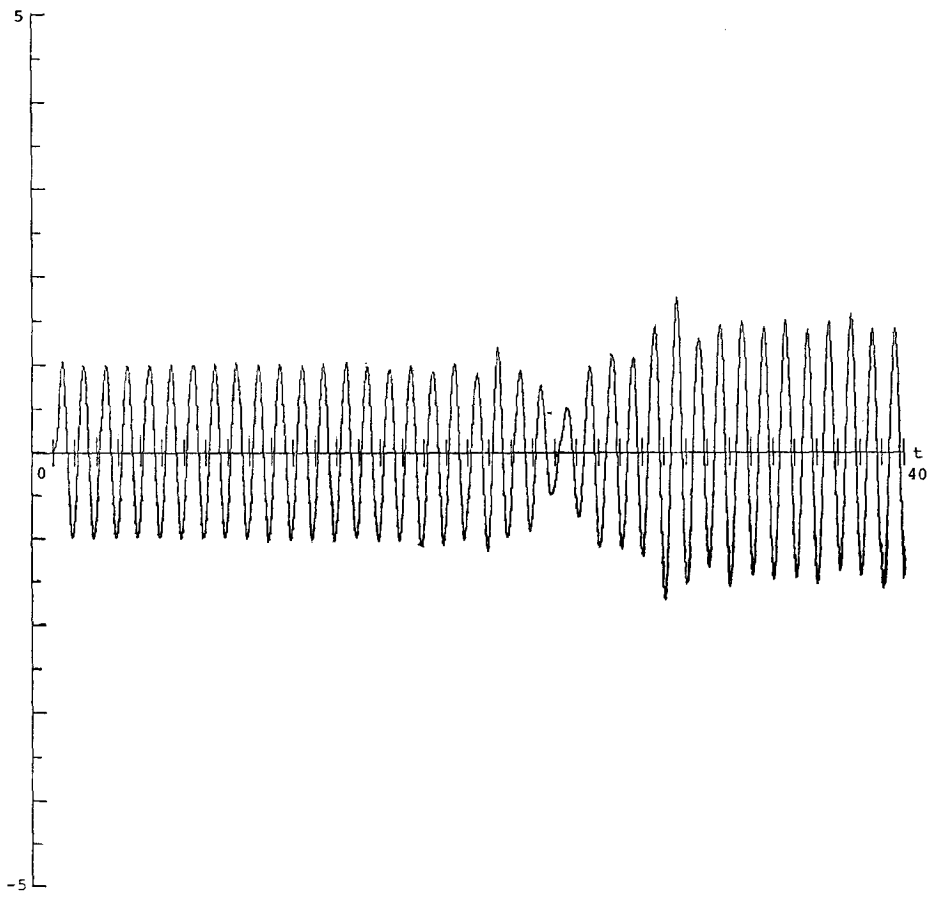

FIG. 7. Plot of the solution to the wave equation (6.1) at $x = -5 \ln 8 \doteq 1.15$ as a function of t using the exponential map with $L = 5$.

These results show that, if high accuracy is desired so $M \gg 1$, then the algebraic map (ii) gives the longest time of accuracy followed by the exponential map (iii) and the restricted domain (i). However, for the cases plotted in Figs. 5–7, the exponential map gives the largest value of t_{accuracy}.

7. BURGERS' EQUATION

In this section we consider the utility of mappings for the problem

$$\frac{\partial u}{\partial t} + u \frac{\partial u}{\partial x} = \nu \frac{\partial^2 u}{\partial x^2} \qquad (0 \leqslant x < \infty, t > 0), \tag{7.1}$$

$$u(x, 0) = f(x), \tag{7.2}$$

$$u(0, t) = g(t). \tag{7.3}$$

Because of the nonlinearity of this problem, there are choices of $f(x)$ and $g(t)$ for which mapping *is* an effective technique to solve the problem numerically and other choices of $f(x)$ and $g(t)$ for which mapping is *not* effective. In general, if the solution approaches a constant as $x \to \infty$ uniformly in t, mapping is effective; if the solution violates this condition, mapping is not effective. We will now give examples to illustrate these remarks.

If $f(x) = e^{-x} - 1$, $g(t) = 0$, then the solution to (7.1)–(7.3) satisfies

$$u(x, t) \sim -\tanh(x/2\nu) \qquad (t \to +\infty). \tag{7.4}$$

For this problem, mapping methods work well. In Fig. 8 we plot the results of numerical integration of (7.1)–(7.3) using a second-order centered difference scheme together with the algebraic map (2.8) with $L = 1$. The results plotted in Fig. 8 illustrate the way in which the asymptotic solution (7.4) is achieved in time.

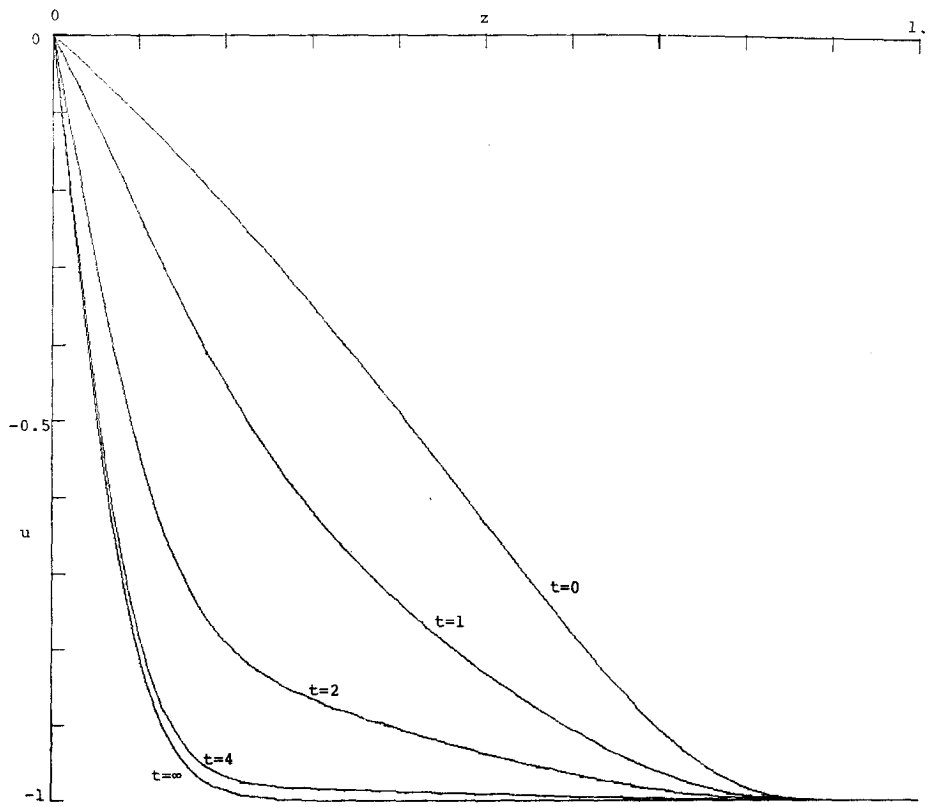

FIG. 8. Plot of the solution to Burgers' equation (7.1) with $u(x, 0) = e^{-x} - 1$ and $u(0, t) = 0$. The problem is solved in the interval $0 \leqslant x < \infty$ using the algebraic map (2.8) with $L = 1$: $z = x/(x + 1)$. The curve labeled $t = \infty$ is the plot of the asymptotic solution (7.4). Here $\nu = .05$ and 101 grid points were used in the interval $0 \leqslant z \leqslant 1$.

On the other hand, if $f(x) = 0$, $g(t) = 1$, then the solution ot (7.1)–(7.3) is given asymptotically by a propagating wave

$$u(x, t) \sim 1 - \tanh[(x - \tfrac{1}{2}t)/2\nu] \qquad (t \to \infty). \tag{7.5}$$

For any of the numerical methods with a fixed grid to treat the boundary at $x = \infty$, there will be a time T beyond which the spatial resolution is not sufficient to reproduce $u(x, t)$ accurately. If the domain is restricted to $0 \leqslant x \leqslant L$, the asymptotic result (7.5) implies that the solution is accurate only for

$$t < 2L.$$

If one of the mappings is used, the solution becomes inaccurate when the shock location at $x = \frac{1}{2}t$ is within a region of poor x resolution. On the basis of the results in Section 6 [see (6.7)], we expect that large errors will result when the shock

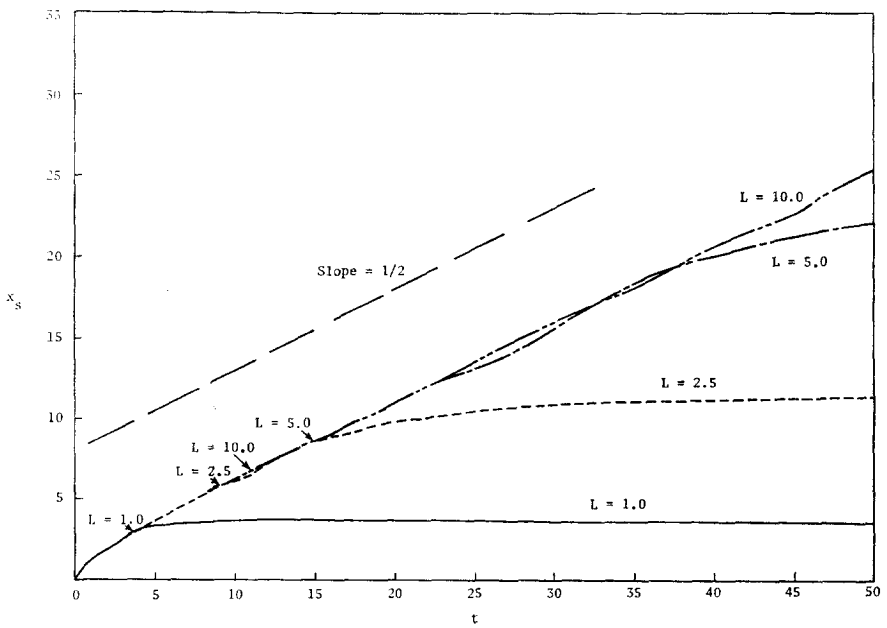

FIG. 9. The position of the shock, x_s, as a function of time, t. The numerical results were obtained with 21 mesh points and the exponential mapping with $L = 1.0, 2.5, 5.0$, and 10.0 and $\nu = 1.0$. The shock position, x_s, is defined by $u(x_s, t) = \frac{1}{2}$. The curves are labeled with the value of L. From Eq. (7.5), the shock speed is $\frac{1}{2}$; the dashed line in the figure has a slope of $\frac{1}{2}$. After a start-up period, $t \approx 1$, the shock propagates with a speed of $\frac{1}{2}$ and then begins to slow down as the mesh spacing increases (see text). The arrows indicate the point at which the shock speed begins to deviate from $\frac{1}{2}$. From Eq. (7.7) the deviation is predicted to occur at $x = 5.9, 12.7, 14.0, 13.9$ for $L = 1.0, 2.5, 5.0$, and 10.0, respectively. The deviation of the shock speed from the value $\frac{1}{2}$ is observed to occur at $x = 3.8, 9.0, 13.0$, and 9.8 for $L = 1.0, 2.5, 5.0$, and 10.0, respectively.

thickness 2ν is larger than Δx. For both the algebraic and exponential maps

$$\frac{dx}{dz} = \frac{L}{(1-z)^{\alpha}},$$

where $\alpha = 1$ for the exponential map and $\alpha = 2$ for the algebraic map. Therefore if $\Delta z = 1/N$, the effective resolution $\Delta x = 2\nu$ when

$$1 - z \approx (L/2N\nu)^{1/\alpha},$$

where we assume that $L \ll 2N\nu$. Thus, the solution using the algebraic map is expected to deteriorate at

$$x_{\text{alg}} \approx 2N\nu(L/2N\nu)^{1/2}, \tag{7.6}$$

while the exponential map should give results that deteriorate near

$$x_{\text{exp}} \approx 2N\nu(L/2N\nu)\ \ln(2N\nu/L). \tag{7.7}$$

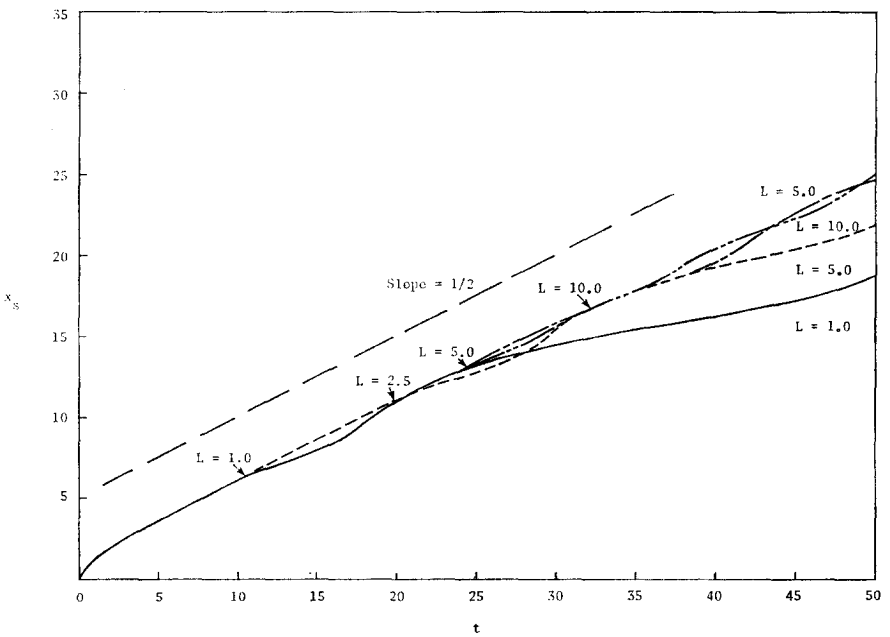

FIG. 10. The position of the shock, x_s, as a function of time, t. The numerical results were obtained using 21 mesh points and the algebraic mapping with $L = 1.0$, 2.5, 5.0, and 10.0 and $\nu = 1.0$. The shock position, x_s, is defined by $u(x_s, t) = \frac{1}{2}$. The curves are labeled with the values of L. From Eq. (7.5) the shock speed is $\frac{1}{2}$; the dashed line in the figure has a slope of $\frac{1}{2}$. After a start-up period, $t \approx 1$, the shock propagates with a speed of $\frac{1}{2}$ and then begins to slow down as the mesh spacing increases (see text). The arrows indicate the point at which the shock speed begins to deviate from $\frac{1}{2}$. From Eq. (7.6) the deviation is predicted to occur at $x = 6.3$, 10.0, 14.1, and 20.0 for $L = 1.0$, 2.5, 5.0, and 10.0, respectively. The deviation of the shock speed from the value $\frac{1}{2}$ is observed to occur at $x = 6.4$, 11.2, 13.0, and 17.0, for $L = 1.0$, 2.5, 5.0, and 10.0, respectively.

Note that (7.6) and 7.7) shows the explicit dependence of x_{alg} and x_{exp} on the small parameter $L/2N\nu$); observe that $x_{exp} \ll x_{alg}$. These predictions are consistent with the results plotted in Figs. 9 and 10.

8. Conclusion

We conclude from the examples given above that mappings are an effective way to solve problems in infinite domains provided that the solution is simple at infinity. If the solution oscillates as $x \to \infty$ then ∞ must be an essential singularity of the solution and mappings fail. Unfortunately, this implies that mappings are nearly useless for many important physical problems.

When mapping is applicable, the proper choice of mapping should be based on the criterion that the solution to the problem be smooth in the mapped coordinate. For many problems this criterion favors algebraic mappings over exponential mappings.

References

1. A. I. van de Vooren and D. Dijkstra, *J. Eng. Math.* **4** (1970), 9.
2. R. T. Davis, *J. Fluid Mech.* **51** (1972), 417.
3. G. K. Batchelor, "An Introduction to Fluid Dynamics," p. 191, Cambridge Univ. Press, London, 1967.
4. S. A. Orszag, *J. Fluid Mech.* **50** (1971), 689.
5. D. Gottlieb and S. A. Orszag, "Numerical Analysis of Spectral Methods: Theory and Applications," Soc. Ind. and Appl. Math., Philadelphia (1977).
6. J. H. Wilkinson, "The Algebraic Eigenvalue Problem," Oxford Univ. Press, London, 1965.
7. R. Jordinson, *Phys. Fluids* **14** (1971), 2535.
8. L. M. Mack, *J. Fluid Mech.* **73** (1976), 497.
9. K. Stewartson, "Theory of Lammar Boundary Layers in Compressible Fluids," Oxford Univ. Press, London, 1964.